

Glucocorticoid Receptor-like Zn(Cys)₄ Motifs in *BsI* Restriction Endonuclease

Éva Scheuring Vanamee¹, Pei-chung Hsieh², Zhenyu Zhu²
David Yates³, Elspeth Garman³, Shuang-yong Xu^{2*} and
Aneel K. Aggarwal^{1*}

¹Structural Biology Program
Department of Physiology
and Biophysics, Mount Sinai
School of Medicine
1425 Madison Avenue
New York, NY 10029, USA

²New England Biolabs, Inc.
32 Tozer Road, Beverly
MA 01915, USA

³Laboratory of Molecular
Biophysics, Department of
Biochemistry, University of
Oxford, Oxford OX1 3QU, UK

BsI restriction endonuclease cleaves the symmetric sequence CCN₇GG (where N = A, C, G or T). The enzyme is composed of two subunits, α and β , that form a heterotetramer ($\alpha_2\beta_2$) in solution. The α subunit is believed to be responsible for DNA recognition, while the β subunit is thought to mediate cleavage. Here, for the first time, we provide experimental evidence that *BsI* binds Zn(II). Specifically, using X-ray absorption spectroscopic analysis we show that the α subunit of *BsI* contains two Zn(Cys)₄-type zinc motifs similar to those in the DNA-binding domain of the glucocorticoid receptor. This conclusion is supported by genetic analysis of the zinc-binding motifs, whereby amino acid substitutions in the zinc finger motifs are demonstrated to abolish or impair cleavage activity. An additional putative zinc-binding motif was identified in the β subunit, consistent with the X-ray absorption data. These data were corroborated by proton induced X-ray emission measurements showing that full *BsI* contains at least three fully occupied Zn sites per α/β heterodimer. On the basis of these data, we propose a role for the *BsI* Zn motifs in protein–DNA as well as protein–protein interactions.

© 2003 Published by Elsevier Ltd.

Keywords: restriction endonuclease; Zn motif; REMS-PCR; microPIXE; EXAFS

*Corresponding authors

Introduction

BsI from *Bacillus species* (strain NEB606) belongs to the type IIT subclass of restriction enzymes (type IIT restriction enzymes are encoded by two restriction genes).¹ *BsI* consists of two subunits: an α subunit of ~26 kDa and a β subunit of ~35 kDa. The *BsI* heterodimer (α/β) dimerizes to form a heterotetramer ($\alpha_2\beta_2$) that recognizes a long interrupted palindromic sequence CCN₇GG (where N is any nucleotide). In DNA mobility-shift assays, neither the α nor the β subunit alone

gave rise to a band shift, indicating that both subunits are required for efficient DNA binding. Individual α or β subunits can be over-expressed in *Escherichia coli* without modification by the corresponding methyltransferase, M. *BsI*, consistent with the idea that the α or β subunit alone lacks the endonuclease activity and is thus not lethal to *E. coli*. *BsI* restriction activity can be reconstituted *in vitro* by combining cell extracts containing α and β subunits, or by combining purified α and β subunits. However, the reconstituted *BsI* endonuclease has lower specific activity, possibly due to aberrant folding and aggregation of the β subunit. The α subunit is believed to be responsible for recognition of the outer base-pairs, while the β subunit binds in the middle and carries the catalytic center for the cleavage of the DNA. *BsI* is one of a handful of restriction enzymes that is thermostable and has been found to remain active even after 20 to 30 cycles of thermal PCR cycling.² Because of its thermostability and its long interrupted recognition sequence, it has been suggested that *BsI* can be used to screen

Abbreviations used: GR, glucocorticoid receptor; ICP-AES, inductively coupled plasma atomic emission spectroscopy; IPTG, isopropyl- β ,D-thiogalactopyranoside; PCR, polymerase chain reaction; REMS-PCR, restriction endonuclease-mediated selective-PCR; PIXE, proton-induced X-ray emission; EXAFS, extended X-ray absorption fine structure; XAS, X-ray absorption spectroscopy; wt, wild-type.

E-mail addresses of the corresponding authors:
xus@neb.com; aggarwal@inka.mssm.edu

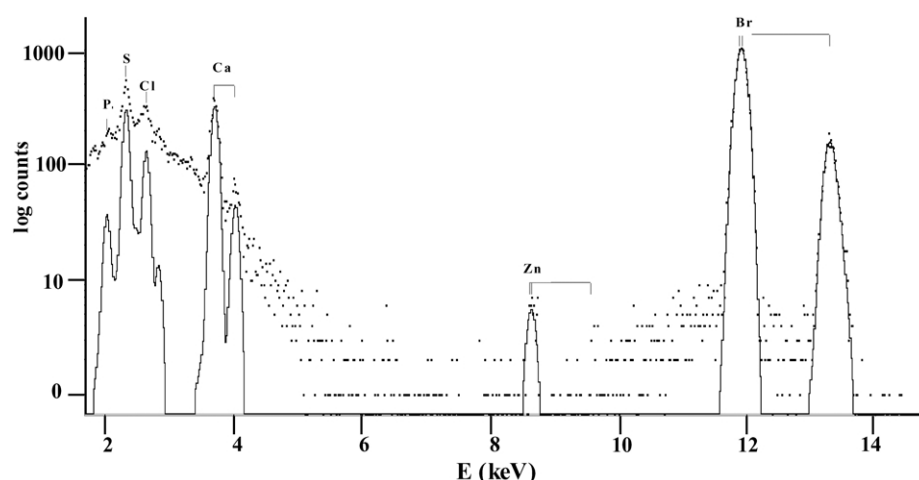


Figure 1. MicroPIXE X-ray spectrum from a point on a sample of *Bsl*I showing elemental peaks present in the sample including sulphur and zinc. The dots represent the experimental data and the solid peaks below the data are the background-subtracted fits.

carcinogenic mutations in a restriction endonuclease-mediated selective-PCR (or REMS-PCR) assay.³ In particular, *Bsl*I could be used to detect the vast majority of mutations that occur at codons 12 or 13 of the *ras* oncogenes (*K-ras*, *H-ras*, and *N-ras*) that encode glycine (codons GGN) at those positions.^{4–6} In an early application of the technique, *Bsl*I was used to detect one tumor cell in a 1000-fold excess of non-diseased cells.³

Here, we provide the first experimental evidence that *Bsl*I binds Zn(II). Zinc-binding motifs were suspected in the α subunit,² on the basis of sequence analysis, but there has been no experimental evidence. Using X-ray absorption spectroscopy (XAS), mutational studies, and proton-induced X-ray emission (microPIXE) spectroscopy, we characterize the Zn(II)-binding sites in *Bsl*I, the first of its kind for a restriction enzyme.

Results

Quantitative zinc analysis

Analysis of full *Bsl*I shows that it contains three or four Zn(II) ions per α/β heterodimer, as determined independently by inductively coupled plasma atomic emission spectroscopy (ICP-AES) and X-ray edge step analysis. Similar analysis of the α subunit alone shows that it binds two Zn(II) ions (Figure 2, inset). To obtain a more accurate measurement of the number of zinc sites in the full enzyme, we used microPIXE analysis. The microPIXE technique applied to elemental analysis of proteins⁷ was used to measure the zinc stoichiometry in two separate liquid samples of full *Bsl*I. The method involves using a 2–3 MeV proton beam of 1 μ m in diameter to induce characteristic

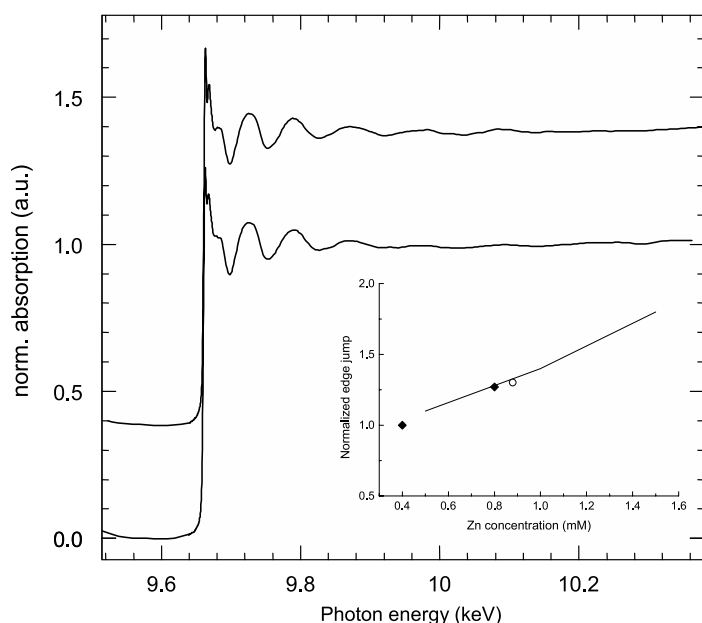


Figure 2. The normalized EXAFS data of the α subunit of *Bsl*I (top) and of the full enzyme (bottom) collected at the zinc K- α edge in fluorescence mode with an energy-resolving Ge detector. The α subunit data is offset for better comparison. The Zn calibration curve is shown in the inset. The edge jump of a 220 μ M full enzyme preparation corresponds to a Zn concentration of 0.9 mM, indicating a 4:1 Zn to protein ratio (open circle). The edge jumps of 200 μ M and 400 μ M α subunit samples correspond to Zn concentrations of 0.4 mM and 0.8 mM, respectively, indicating a 2:1 Zn to protein ratio (filled diamonds).

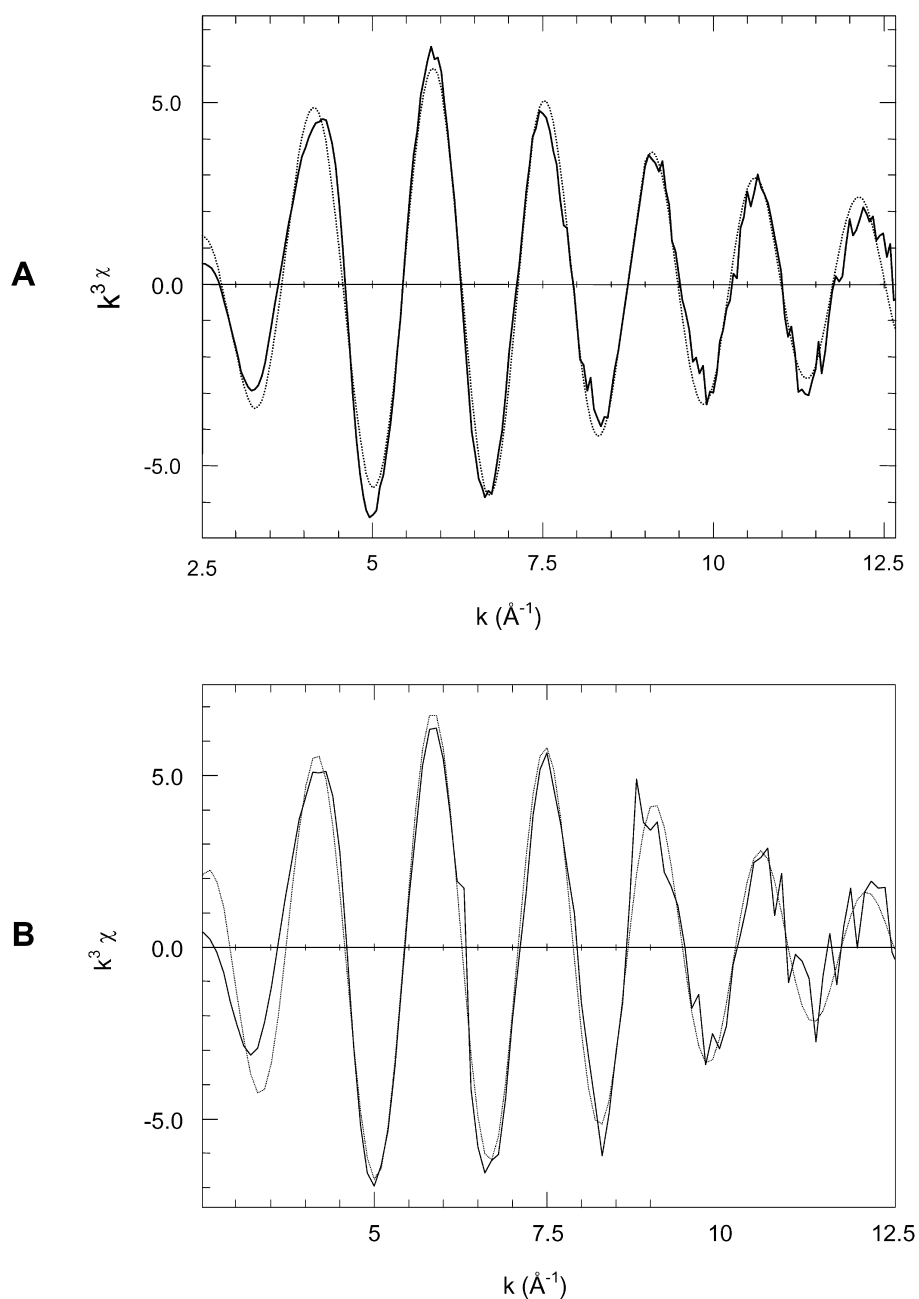


Figure 3. A, The unfiltered k^3 -weighted χ data of the α subunit (continuous line). The best fit (shown with a dotted line) provides Zn–S distances of 2.27(2) Å and 2.37(3) Å with a χ^2 value of 1.8. B, The unfiltered k^3 -weighted χ data of the full enzyme (continuous line) and the simulated data (dotted line) using 3.5 S + 0.5 N contribution. The fit provides a Zn–S distance of 2.33(2) Å and a Zn–N distance of 2.01(2) Å with a χ^2 value of 1.5.

X-ray emission from protein crystals or solution dried onto a mylar film held in vacuum. These characteristic X-rays are then detected in a solid-state, lithium-drifted silicon detector with high-energy resolution. Figure 1 shows a microPIXE point spectrum of full *BslI*. The zinc content was computed by internal calibration to the sulfur content of the samples. Analysis of three point spectra for two different sample preparations gave an average number of zinc atoms per *BslI* α/β heterodimer molecule of 3.6(\pm 0.5). A control point spectrum was run on the buffer and the mylar foil

and no zinc or sulfur was detected. In summary, the microPIXE results clearly show that the full *BslI* α/β heterodimer contains at least three fully occupied Zn sites and possibly a fourth site as well.

X-ray absorption spectroscopic results

To structurally characterize the zinc-binding sites in *BslI*, we used extended X-ray absorption fine structure (EXAFS) analysis. EXAFS is a powerful technique to probe the local environment of metal centers in solution, and it has proven to be

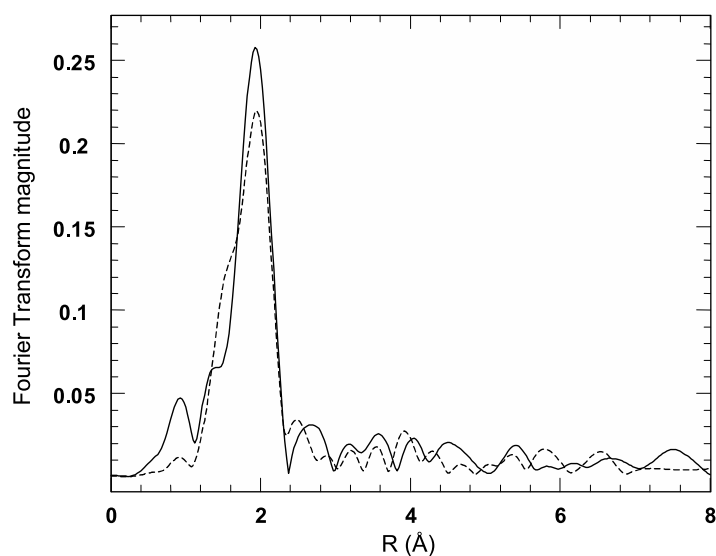


Figure 4. The Fourier-transformed data of the α subunit of *Bsl I* (continuous line) and the full enzyme (broken line).

especially useful in providing structural details about Zn(II)-binding proteins where other spectroscopic methods have failed. EXAFS data of the α subunit of *Bsl I* measured at the Zn K edge are shown in Figure 2 (top). The edge jump is consistent with a 2:1 zinc to protein ratio. Figure 3A shows the background-subtracted and k^3 -weighted χ data that represent the sum of all scattering contribution from atoms around the zinc center. The Fourier-transformed data are shown in Figure 4. The largest peak corresponds to the scattering contribution from the nearest or first-shell atoms around the zinc center. Detailed analysis, to determine the nature and number of ligands, was carried out on the unfiltered k^3 -weighted χ data. The least-squares fitting results are summarized in Table 1. The one atom type 4S fit provides a reduced χ^2 value of 1.9. The 3S type fit provides a χ^2 value that is more than twice that of the 4S type fit. Also, letting the coordination number float during the fit results in a coordination number of

Table 1. Non-linear, least-squares fitting results of the α subunit of *Bsl I*

Number of ligands	Type of ligand	Distance (Å)	$\Delta\sigma^2$ (Å ²)	χ^2
4	Zn-S	2.33 ± 0.02	0.005	1.9
3	Zn-S	2.33 ± 0.02	0.004	4.3
2	Zn-S	2.27 ± 0.02	0.003	1.8
2	Zn-S	2.37 ± 0.02	0.004	
3.5	Zn-S	2.33 ± 0.02	0.005	2.3
0.5	Zn-N	2.01 ± 0.01	-0.0001	
3	Zn-S	2.33 ± 0.02	2.7	0.004
1	Zn-N	2.03 ± 0.02	0.001	
2	Zn-S	2.37 ± 0.02	0.003	4.3
2	Zn-N	2.05 ± 0.02	0.001	

$S_0^2 = 1.1$; $\Delta E_0 = 4.5$, $\Delta k = 10$, where S_0^2 is the amplitude reduction factor, ΔE_0 is the shift in the threshold energy, and Δk is the range of data used in the fitting. The best fit is highlighted in bold.

4.1. Together, these results support tetrahedral coordination around the Zn(II) ion.

The best fit is (Figure 3A, dotted line) provided with the two atom type 2S:2S fit with a χ^2 value of 1.8. The mixed sulfur nitrogen type fits all give worse χ^2 values than that of the 2S:2S type fit. Moreover, the existence of two 2S:2N type or two 3S:1N Zn sites are not supported by the data, though the presence of a His ligand cannot be ruled out. Including Zn-Zn contribution within 4 Å did not provide acceptable fitting results, making the presence of a Zn₂Cys₆-type motif unlikely. Together, the EXAFS results from the α subunit indicate the existence of two ZnCys₄ type zinc motifs in the α subunit. By sequence, residues C36, C39, C50, and C53 likely comprise zinc motif I, while C63, C66, C79, and C84 correspond to motif II.

The EXAFS fitting results for the full α/β enzyme are summarized in Table 2. The major difference in comparing the fitting results for the

Table 2. Non-linear, least-squares fitting results of full *Bsl I*

Number of ligands	Type of ligand	Distance (Å)	$\Delta\sigma^2$ (Å ²)	χ^2
4	Zn-S	2.32 ± 0.02	0.007	1.8
3	Zn-S	2.33 ± 0.02	0.004	4.3
2	Zn-S	2.36 ± 0.02	0.002	1.7
2	Zn-S	2.31 ± 0.02	0.009	
3.5	Zn-S	2.33 ± 0.02	0.006	1.5
0.5	Zn-N	2.01 ± 0.01	0.001	
3	Zn-S	2.33 ± 0.02	0.005	1.7
1	Zn-N	2.02 ± 0.02	0.003	
2	Zn-S	2.33 ± 0.02	0.002	3.3
2	Zn-N	2.04 ± 0.02	0.001	

$S_0^2 = 1.1$; $\Delta E_0 = 4.5$, $\Delta k = 10$, where S_0^2 is the amplitude reduction factor, ΔE_0 is the shift in the threshold energy, and Δk is the range of data used in the fitting. The best fit is highlighted in bold.

α subunit is that the best fit is obtained with a 3.5S:0.5N ratio with the 2S:2S and 3S:1N-type fits being close second. The presence of all 2S:2N-type motifs are unlikely, considering the EXAFS results. This indicates that in addition to the two ZnCys₄ type Zn(II) sites present in the α subunit, one or two mixed Cys and His-containing zinc motifs may be present in the full enzyme. The EXAFS characterization of the β subunit alone however, was hampered by precipitation even at low concentrations. Correspondingly, using dynamic light-scattering studies we found that the β subunit forms aggregates in the absence of the α subunit at relatively low concentrations. Furthermore, a cleavage assay showed that the β subunit does not bind or cleave DNA on its own, suggesting that the β subunit is unstable by itself.

Mutagenesis of zinc-binding motifs in the α and β subunits

As a complement to the biophysical data, we undertook a genetic interrogation of the suspected zinc-binding residues. From the random mutagenesis, a *Bsl*I variant C53R of the α subunit was isolated that lost *Bsl*I cleavage activity. Since residue C53 is located in the putative Zn(II)-binding motif I,² additional *Bsl*I variants were constructed in order to understand the contribution of the Cys residues in the two putative Zn(II)-binding sites.² By site-directed mutagenesis, eight *Bsl*I variants were constructed, including C36A, C39A, C50A,

C53A, C63A, C66A, C79A, and C84A. IPTG-induced cell extracts with the mutant α subunit were reconstituted with wild-type (wt) β subunit extract and *Bsl*I activity was assayed on pUC19 DNA. Two variants, C50A (zinc motif I), and C63A (zinc motif II) displayed complete loss of enzymatic activity (less than 0.1% of wt activity). The C36A, C39A, and C53A variants had partial activities (~10% wt activity), while the C66A, C79A and C84A variants exhibited near-wt activities (~50% wt activity). The cleavage activity results are summarized in Table 3. In cases where the mutant subunit from crude extracts did not display endonuclease activity after enzyme reconstitution, an affinity purification step was conducted to ensure that the expression of protein was not the factor giving the negative activity result. Interestingly, the C53R mutant was inactive as compared to C53A, which had partial activity, suggesting that the long, positively charged side-chain of the Arg distorts the Zn(II)-binding site more severely than the smaller and neutral Ala residue.

Interestingly, the β subunit contains a C62-X₃-H66-X₁₂-C79-X₂-C82 sequence that may comprise an additional zinc motif III. This would be consistent with the EXAFS and microPIXE results, suggesting additional zinc-binding outside of the α subunit. To test this, four β subunit variants, β C62K, β H66K, β C79K and β C82K, were isolated by site-directed mutagenesis. Cell extracts with mutated β subunit were complemented with wt α subunit cell extract and *Bsl*I cleavage activity was assayed on pUC19 DNA. *Bsl*I variants containing β C62K, β C79K and β C82K displayed impaired cleavage activity (approximately tenfold reduction in cleavage activity). The *Bsl*I variant with mutated subunit β H66K displayed near-wt enzymatic activity. While the purified α subunit mutants have very similar yields compared to the yield of wt α , the protein yields of the β subunit mutants are five to six times lower than that of the wt β subunit. This indicates that the β subunit mutants are impaired in protein folding more severely compared to the α subunit mutants. All active mutants have the same cleavage pattern as that of the wt enzyme, indicating that the mutations do not affect specificity.

In summary, mutations in motif I of the α subunit affect enzymatic function strongly, while mutations in motif II are less disruptive, indicating that the two Zn-binding sites have different roles in the folding and stability of the enzyme. Interestingly, both motifs share sequence homology with Krüppel-type zinc binding.² The genetic data support the conclusion derived from EXAFS measurements that there are two Zn(II) ions per α subunit that are most likely bound in Zn(Cys)₄-type motifs. The mutational analysis of the putative zinc motif III in the β subunit is consistent with EXAFS, indicating a third mixed Cys and His-containing motif in *Bsl*I endonuclease.

Table 3. Cleavage activity of *Bsl*I mutants

Mutants	Protein in	<i>Bsl</i> I cleavage activity	Location in
A. α Subunit			
C36A	Crude extract	~10%	Zn ²⁺ motif I ^a
C39A	Crude extract	~10%	Zn ²⁺ motif I
C50A	Purified	<0.1%	Zn ²⁺ motif I
C53A	Crude extract	~10%	Zn ²⁺ motif I
C53R	Purified	<0.1%	Zn ²⁺ motif I
C63A	Purified	<0.1%	Zn ²⁺ motif II ^b
C66A	Crude extract	~50%	Zn ²⁺ motif II
C79A	Crude extract	~50%	Zn ²⁺ motif II
C84A	Crude extract	~50%	Zn ²⁺ motif II
B. β Subunit			
β C62K	Purified	<0.1%	Zn ²⁺ motif III ^c
β H66K	Crude extract	~50%	Zn ²⁺ motif III
β C79K	Purified	~10%	Zn ²⁺ motif III
β C82K	Purified	~10%	Zn ²⁺ motif III

^a α Subunit Zn²⁺ motif I, C36-X₂-C39-X₁₀-C50-X₂-C53.

^b α Subunit Zn²⁺ motif II, C63-X₂-C66-X₁₂-C79-X₄-C84.

^c β -Subunit Zn²⁺ motif III, C62-X₃-H66-X₁₂-C79-X₂-C82.

Discussion

The results here provide the first experimental evidence that *BslI* binds zinc. The EXAFS data of the α subunit are consistent with the presence of tetrahedral ZnCys_4 -type zinc motifs. Importantly, the EXAFS data do not support the presence of a Zn_2Cys_6 -type zinc cluster found in GAL4.⁸ Moreover, the presence of two $\text{ZnCys}_3\text{His}_1$ or two $\text{ZnCys}_2\text{His}_2$ -type zinc motifs is also unlikely, on the basis of the EXAFS results, and is not supported by primary sequence analysis. In contrast, the EXAFS data of the full protein are most consistent with mixed Cys His coordination. Taken together, the EXAFS results suggest that *BslI* most likely contains two ZnCys_4 -type Zn motifs in the α subunit and an additional mixed Cys His Zn motif in the β subunit. These results are supported by mutagenesis, microPIXE, and sequence alignment analyses.

Interestingly, among the more than 3500 type II restriction enzymes isolated to date,⁹ only a few have been suspected to bind Zn; namely, *BslI*,² *SapI*, *HpyI*,¹⁰ and *PacI* (R. Morgan & S.-y.X., unpublished results). In contrast, Zn(II)-binding motifs are common in DNA-binding transcription factors and RNA-binding translational regulators.^{11–14} Zinc motifs have been discovered in a number of nucleases, including intron-encoded endonuclease *I-PpoI* and *I-TevI*,^{15,16} non-specific colicin endonuclease of the HNH superfamily,¹⁷ and the DNA repair enzyme endonuclease IV.¹⁸ The Zn(II) ions play a structural role in folding of nuclease *I-PpoI*, *I-TevI* and colicin endonuclease, and may play a catalytic role in the AP endonuclease IV. Zn(II) motifs I and II in *BslI* are an all-Cys variation of the Krüppel Cys2His2-type Zn finger motif that is so prevalent in eukaryotic transcription factors but so far has not been found in bacterial restriction endonucleases. Despite no sequence homology, we find strong structural and functional similarities between the Zn(II) sites of the α subunit and that of the glucocorticoid receptor (GR), which contains a DNA-binding domain with two Zn(II) motifs. Similar to our data for the α subunit, the EXAFS data for GR reflect a tetrahedral ZnCys_4 coordination,¹⁹ that was confirmed later by crystallographic analysis.²⁰ In addition, the calculated Zn–S distances of 2.33(2) Å for motif I and motif II in *BslI* are the same, within error, as those found for GR (2.32(2) Å). In GR, the two $\text{Zn}(\text{Cys})_4$ sites have different roles, one participates in protein–DNA interactions and the other in protein–protein interactions. Similarly, in the α subunit of *BslI*, which is believed to bind specifically to the outer two cytosine bases of the recognition sequence (Figure 5), one of the Zn(II) motifs may participate in protein–DNA interactions and the other might mediate protein–protein interactions, although better understanding will derive from full structural analysis. Interestingly, the mutagenesis results showed a smaller effect on the enzymatic activity by the Cys mutations in motif



Figure 5. A representation of the subunit arrangement of *BslI* bound to its recognition sequence. The α subunits are responsible for recognition of the outer cytosine bases and the β subunits cleave between the recognition sites indicated by the arrows.

II reflecting differing roles for motif I and motif II in the structural and functional integrity of the enzyme. This kind of disparity between Zn finger sites is not unusual. Similar behavior has been found in several RING domains. As an example, the arenaviral protein Z contains two Zn-binding sites that form a RING domain. Wild-type Z forms spherical structures, and the self-assembly of these structures depends on an intact RING domain. Mutations in the first Zn-binding site result in a partially folded protein that does not self-assemble. However, even a Cys to Ala double mutation of the last two residues in site 2 results in a mutant that is fully folded and whose self-assembly and biological function resembles closely that of wt Z.²¹

The instability of the β subunit has implications for the function of *BslI*. The β subunit carries the catalytic center and it cleaves non-specifically between the outer bases recognized by the two α subunits (Figure 5). Without a safeguarding mechanism, the β subunit would cleave DNA indiscriminately, which would result in self-destruction. By ensuring that the β subunit becomes activated only in the presence of the α subunit, non-specific cleavage can be avoided. The α/β interface likely plays an important role in controlling the proper folding and activity of the enzyme. In all, the experimental evidence for Zn(II) in *BslI* and the detailed characterization of the Zn(II)-binding sites here are the first of its kind for a restriction endonuclease.

Experimental Procedures

Random and site-directed mutagenesis

To create random mutations on the *BslI* endonuclease gene, we used the Taq DNA polymerase under the conditions of 35 cycles of one minute at 95 °C, one minute at 55 °C, and two minutes at 72 °C in PCR. The amplified products were cloned into pAII17 plasmid (a pET derivative) and transformed into ER2566 without M. *BslI* protection. Survivor transformants were expected to contain mutation(s) in the endonuclease genes *bslI* α or *bslI* β . The plasmid DNA was isolated from the surviving colonies followed by restriction mapping. The colonies that carried the desired size insert (1.4 kb) of *BslI* endonuclease genes were selected. The crude extracts of these selected colonies were analyzed by SDS-PAGE and the proteins transferred onto a polyvinylidene fluoride (PVDF) membrane. Rabbit polyclonal

antibody against the α and β subunit of BslI endonuclease was used for the detection of the protein of the desired size.

Site-directed mutagenesis was carried out by PCR using four primers as described.²² PCR reaction 1 was carried out with forward N-terminal primer and mutagenic reverse primer, and PCR reaction 2 was performed with forward mutagenic primer and reverse C-terminal primer. The two PCR products were gel-purified, combined, and reamplified with forward N-terminal and reverse C-terminal primers. All mutagenic PCR primers were synthesized at New England Biolabs' organic synthesis laboratory.

DNA manipulation

Plasmid DNA isolation was by Qiagen spin column or tip-20 column. Plasmid DNA containing the mutant alleles was sequenced by the dideoxy termination method using the AmpliTaq dideoxy terminator sequencing kit and an ABI373A sequencing machine.

Protein expression and activity assay

Full BslI, and its α and β subunits were expressed and purified as described.² For detection of individual subunit mutants, the BslI endonuclease was reconstituted *in vitro* by incubating mutant α with the wt β subunit or mutant β with the wt α subunit at 37 °C for an hour followed by digestion of DNA substrate. Cleavage assay was carried out in NEBuffer 3 (100 mM NaCl, 50 mM Tris-HCl, 10 mM MgCl₂, 1 mM DTT) at 55 °C for one hour on pUC19 DNA or λ DNA. All mutant alleles were sequenced using the dye terminator sequencing kit from Applied Biosystems.

Quantitative zinc analysis

The zinc content of samples was determined by several techniques. First, ICP-AES was performed at Galbraith Laboratories, Knoxville, TN. Prior to measurement, the samples were digested with nitric acid. Second, XAS edge step analysis was carried out by comparing the edge step of the samples to calibration standards with known concentration. Finally, microPIXE with a scanning proton microprobe was used to find the elemental composition.⁷ The microPIXE experiments were carried out on the proton microbeam at the University of Surrey Center for Research in Ion Beam Applications, Guildford, UK. Prior to analysis, the protein samples were exchanged into a buffer containing 20 mM Tris, 0.1 M NaBr and 0.1 M EDTA to avoid the presence of additional sulfur and chloride that would interfere with the measurements. Two samples at different concentrations (3–4 mg/ml and ~1 mg/ml) were analyzed. Three 0.2 μ l drops of each preparation were placed onto two separate 2 μ m thick mylar films (one for each preparation), each of which had been pre-tensioned over a 1 cm hole in an aluminum target holder and then the film was glued to the holder. A 2 MeV proton beam was used for the measurements. For each preparation and for the buffer, quantitative information was obtained by collecting spectra for five minutes each at three or four points on a dried drop of each and on the backing foil alone. These spectra were analyzed using GUPIX²³ to extract the concentration of each element of interest in the sample. The number of zinc atoms per protein molecule was computed from the ratio of zinc to the sulfur measurements with knowledge of

the sulfur content of the protein from the primary sequence. This internal sulfur calibration allows much more accurate quantification (normally approx. \pm 10%, best \pm 6%) than would be possible if absolute measurements were necessary.

X-ray absorption data collection and analysis

Samples for XAS data collection were concentrated and then resuspended in 100 mM potassium phosphate (pH 7.5), 150 mM NaCl, 30% (v/v) glycerol. The final concentration of the full enzyme was 220 μ M and the concentration of the α subunit was 450 μ M as determined by UV absorption at 280 nm. A sample (50–70 μ l) was loaded into a 0.5 mm thick copper sample-holder with a 10 mm \times 5 mm hole in the center covered with mylar tape. The samples were frozen over liquid nitrogen before data collection.

XAS data were collected at the National Synchrotron Light Source (NSLS), Brookhaven National Laboratory (Upton, NY), on beamline X-9B using a sagittally focused Si[111] crystal monochromator. A Ni mirror at an angle of 4.5 mrad was used to reject higher-order harmonic contamination. All experiments were carried out at 70 K in a closed cycle He cryostat under vacuum. EXAFS data were collected with 0.05 \AA^{-1} step sizes in k space starting at 1 \AA^{-1} photoelectron energy. The signal averaging was weighted with respect to k , so that 2 s per point was used at $k = 1$ and 7 s per point was used at $k = 14$. Below 1 \AA^{-1} , data were collected by counting at a specific energy for 1 s and incrementing the energy by 10 eV from 150 eV below the zinc edge to 20 eV below the edge, then in 2.0 eV steps up to 1 \AA^{-1} with 1 s per point signal averaging. Edge data were collected in three regions; from 150 eV to 20 eV below the edge position with 10 eV steps and 1 s per point signal averaging, then from 20 eV below the edge to 20 eV above the edge with 0.5 eV steps and 2 s per point signal averaging, and finally from 20 eV to 200 eV above the edge with 1 eV steps and 2 s per point signal averaging. Three to five edge scans were recorded for each sample. To reduce the possibility of sample degradation, several independently prepared samples were measured for each compound. Data were generally taken in the range of 150–250 mA beam current. K- α Zn fluorescence was detected at a 90° angle from the incident beam using a 13 element energy-resolving Ge detector.²⁴ The internal count rates were kept at or less than 30,000/s per channel to avoid saturation effects in the detector. A calibration channel behind the sample was set up to detect the spectrum of a Zn foil simultaneously with all sample spectra. This calibration channel provided a reference for the energy calibration of the sample spectra; the K-edge inflection point assigned as 9659 eV.

Data manipulation with use of a linear pre-edge fit, cubic polynomial spline background subtraction, wave-vector cubed weighting, and Fourier transformation were performed using the WinXAS package²⁵ on an IBM-compatible machine running under Microsoft Windows 98.

The theoretical data were generated using the *ab initio* code FEFF (v 6.01).^{26,27} The coordinates of zinc models were extracted from known crystal structures deposited in the Protein Data Bank using a 5 \AA radius around the Zn(II) ion. The Zn₂Cys₆ model was taken from the structure of Gal4,⁸ the ZnCys₄ model was generated from the structure of the glucocorticoid receptor,²⁰ and the mixed Cys, His contributions were generated from the structure

of Zif268.²⁸ In the FEFF input file, only a few parameters were adjusted, such as the amplitude reduction factor (S_0^2) and the number of scattering paths (NLEG). The Debye–Waller parameter (σ^2) was disabled in FEFF in order to be adjusted during the fitting procedure.

The theoretical data are fit to the unfiltered experimental k^3 weighted χ data using the non-linear, least-squares method implemented in WinXAS by fixing the coordination number (N) and the shift in the threshold energy ΔE_{∞} , and letting the distance (r) and σ^2 to float. The goodness of fit (χ^2) is given in the form of a weighted residual sum squared:

$$\chi^2 = \frac{\sum_i \{(k^3\chi_i)_{\text{experimental}} - (k^3\chi_i)_{\text{simulation}}\}^2}{100\sqrt{N}} \quad (1)$$

where N is the number of data points.

Only those minima with reasonable σ^2 values ($\leq \pm 0.01$) are accepted as possible solutions. The final results are presented in Tables 1 and 2 for the α subunit and for full Bsl I, respectively.

Acknowledgements

We thank Michael Sullivan for helping with XAS data collection at beamline X9B and Geoff Grime for assistance with microPIXE measurements. We thank Kathy Borden and the anonymous reviewers for helpful suggestions. The construction and operation of beamline X9B is supported by the Biotechnology Research Resource program of the National Institute of Health. The NSLS is supported by the Department of Energy, Division of Materials Sciences, Office of Energy Research. This work was supported by National Institute of Health grants GM44006 (to A.K.A.), and GM20015 (to É.S.V.).

References

- Pingoud, A. & Jeltsch, A. (2001). Structure and function of type II restriction endonucleases. *Nucl. Acids Res.* **29**, 3705–3727.
- Hsieh, P. C., Xiao, J. P., O’Loane, D. & Xu, S. Y. (2000). Cloning, expression, and purification of a thermostable nonhomodimeric restriction enzyme, Bsl I. *J. Bacteriol.* **182**, 949–955.
- Fuery, C. J., Impey, H. L., Roberts, N. J., Applegate, T. L., Ward, R. L., Hawkins, N. J. *et al.* (2000). Detection of rare mutant alleles by restriction endonuclease-mediated selective-PCR: assay design and optimization. *Clin. Chem.* **46**, 620–624.
- Almoguera, C., Shibata, D., Forrester, K., Martin, J., Arnheim, N. & Perucho, M. (1988). Most human carcinomas of the exocrine pancreas contain mutant c-K-ras genes. *Cell*, **53**, 549–554.
- Bos, J. L. (1989). ras oncogenes in human cancer: a review. *Cancer Res.* **49**, 4682–4689.
- Vogelstein, B., Fearon, E. R., Hamilton, S. R., Kern, S. E., Preisinger, A. C., Leppert, M. *et al.* (1988). Genetic alterations during colorectal-tumor development. *N. Engl. J. Med.* **319**, 525–532.
- Garman, E. (1999). Leaving no element of doubt: analysis of proteins using microPIXE. *Struct. Fold. Des.* **7**, R291–R299.
- Marmorstein, R., Carey, M., Ptashne, M. & Harrison, S. C. (1992). DNA recognition by GAL4: structure of a protein–DNA complex. *Nature*, **356**, 408–414.
- Roberts, R. J., Vincze, T., Posfai, J. & Macelis, D. (2003). REBASE: restriction enzymes and methyltransferases. *Nucl. Acids Res.* **31**, 418–420.
- Bujnicki, J. M., Radlinska, M. & Rychlewski, L. (2001). Polyphyletic evolution of type II restriction enzymes revisited: two independent sources of second-hand folds revealed. *Trends Biochem. Sci.* **26**, 9–11.
- Laity, J. H., Lee, B. M. & Wright, P. E. (2001). Zinc finger proteins: new insights into structural and functional diversity. *Curr. Opin. Struct. Biol.* **11**, 39–46.
- Wolfe, S. A., Nekludova, L. & Pabo, C. O. (2000). DNA recognition by Cys2His2 zinc finger proteins. *Annu. Rev. Biophys. Biomol. Struct.* **29**, 183–212.
- Khorasanizadeh, S. & Rastinejad, F. (2001). Nuclear-receptor interactions on DNA-response elements. *Trends Biochem. Sci.* **26**, 384–390.
- Low, L. Y., Hernandez, H., Robinson, C. V., O’Brien, R., Grossmann, J. G., Ladbury, J. E. & Luisi, B. (2002). Metal-dependent folding and stability of nuclear hormone receptor DNA-binding domains. *J. Mol. Biol.* **319**, 87–106.
- Flick, K. E., Jurica, M. S., Monnat, R. J., Jr & Stoddard, B. L. (1998). DNA binding and cleavage by the nuclear intron-encoded homing endonuclease I-PpoI. *Nature*, **394**, 96–101.
- Van Roey, P., Waddling, C. A., Fox, K. M., Belfort, M. & Derbyshire, V. (2001). Intertwined structure of the DNA-binding domain of intron endonuclease I-TevI with its substrate. *EMBO J.* **20**, 3631–3637.
- Pommer, A. J., Kuhlmann, U. C., Cooper, A., Hemmings, A. M., Moore, G. R., James, R. & Kleantous, C. (1999). Homing in on the role of transition metals in the HNH motif of colicin endonucleases. *J. Biol. Chem.* **274**, 27153–27160.
- Hosfield, D. J., Guan, Y., Haas, B. J., Cunningham, R. P. & Tainer, J. A. (1999). Structure of the DNA repair enzyme endonuclease IV and its DNA complex: double-nucleotide flipping at abasic sites and three-metal-ion catalysis. *Cell*, **98**, 397–408.
- Freedman, L. P., Luisi, B. F., Korszun, Z. R., Basavappa, R., Sigler, P. B. & Yamamoto, K. R. (1988). The function and structure of the metal coordination sites within the glucocorticoid receptor DNA binding domain. *Nature*, **334**, 543–546.
- Luisi, B. F., Xu, W. X., Otwinowski, Z., Freedman, L. P., Yamamoto, K. R. & Sigler, P. B. (1991). Crystallographic analysis of the interaction of the glucocorticoid receptor with DNA. *Nature*, **352**, 497–505.
- Kentsis, A., Gordon, R. E. & Borden, K. L. (2002). Self-assembly properties of a model RING domain. *Proc. Natl. Acad. Sci. USA*, **99**, 667–672.
- Morrison, H. G. & Desrosiers, R. C. (1993). A PCR-based strategy for extensive mutagenesis of a target DNA sequence. *Biotechniques*, **14**, 454–457.
- Johansson, S. A. E., Campbell, J. L. & Malmquist, K. G. (1995). *Particle Induced X-ray Emission Spectrometry*, Wiley, New York.
- Cramer, S. P., Chen, E., George, S. J., van Elp, J., Moore, J., Tensch, O. *et al.* (1992). Soft X-ray spectroscopy of metalloproteins using fluorescence detection. *Nucl. Instrum. Methods sect. A*, **319**, 289–295.

25. Ressler, T. (1998). WinXAS: a program for X-ray absorption data analysis under MS-Windows. *J. Synchrotron Rad.* **5**, 118–122.
26. Rehr, J. J., Mustre de Leon, J., Zabinsky, S. I. & Albers, R. C. (1991). Theoretical X-ray absorption fine structure standards. *J. Am. Chem. Soc.* **113**, 5135–5140.
27. Rehr, J. J., Albers, R. C. & Zabinsky, S. I. (1992). High-order multiple-scattering calculations of X-ray-absorption fine structure. *Phys. Rev. Letters*, **69**, 3397–3400.
28. Pavletich, N. P. & Pabo, C. O. (1991). Zinc finger-DNA recognition: crystal structure of a Zif268-DNA complex at 2.1 Å. *Science*, **252**, 809–817.

Edited by J. O. Thomas

(Received 2 June 2003; received in revised form 16 September 2003; accepted 19 September 2003)